Proper Generalized Decomposition solution of the parameterized Helmholtz problem: application to inverse geophysical problems.

Marianna Signorini*[1], Sergio Zlotnik[2] and Pedro Díez[2]

[1] *MOX– Modellistica e Calcolo Scientifico, Dipartimento di Matematica "F. Brioschi", Politecnico di Milano*
[2] *Laboratori de Càlcul Numèric (LaCàN), Universitat Politècnica de Catalunya, Jordi Girona 1, E-08034 Barcelona, Spain*

SUMMARY

The identification of the geological structure from seismic data is formulated as an inverse problem. The properties and the shape of the rock formations in the subsoil are described by material and geometric parameters, which are taken as input data for a predictive model. Here, the model is based on the Helmholtz equation, describing the acoustic response of the system for a given wave length. Thus, the inverse problem consists in identifying the values of these parameters such that the output of the model agrees the best with observations. This optimization algorithm requires multiple queries to the model with different values of the parameters. Reduced Order Models are especially well suited to significantly reduce the computational overhead of the multiple evaluations of the model.
In particular, the Proper Generalized Decomposition (PGD) produces a solution explicitly stating the parametric dependence, where the parameters play the same role as the physical coordinates. A PGD solver is devised to inexpensively explore the parametric space along the iterative process. This exploration of the parametric space is in fact seen as a post-process of the generalized solution. The approach adopted demonstrates its viability when tested in two illustrative examples.

KEY WORDS: parameterized Helmholtz problem; Proper Generalised decomposition (PGD); parameter identification; inverse problems; seismic analysis

INTRODUCTION

Seismic inversion and parameter identification is a very important task in geophysics. In particular, geologists are interested in understanding subsoil structures and layers, especially their physical properties and dimensions. These properties are usually inferred from acoustic data, originated from land or marine surveys. Different inversion techniques have been developed during the years in order to deal with this problem [1, 2, 3].

The pressure field produced during the explorations is typically modelled with the transient wave equation and the inversion is performed via the minimization of a suitable functional depending on the records of the waves on the ground surface. We consider the Helmholtz equation in order to properly describe the stationary pressure field during a seismic survey performed, for example, with the vibroseis technique. The Helmholtz equation describes the phenomenon in a steady state case

*Correspondence to: Marianna Signorini, marianna.signorini@polimi.it

Contract/grant sponsor: Spanish Ministry of Economy and Competitiveness; contract/grant number: CICYT-DPI2014-51844-C2-2-R

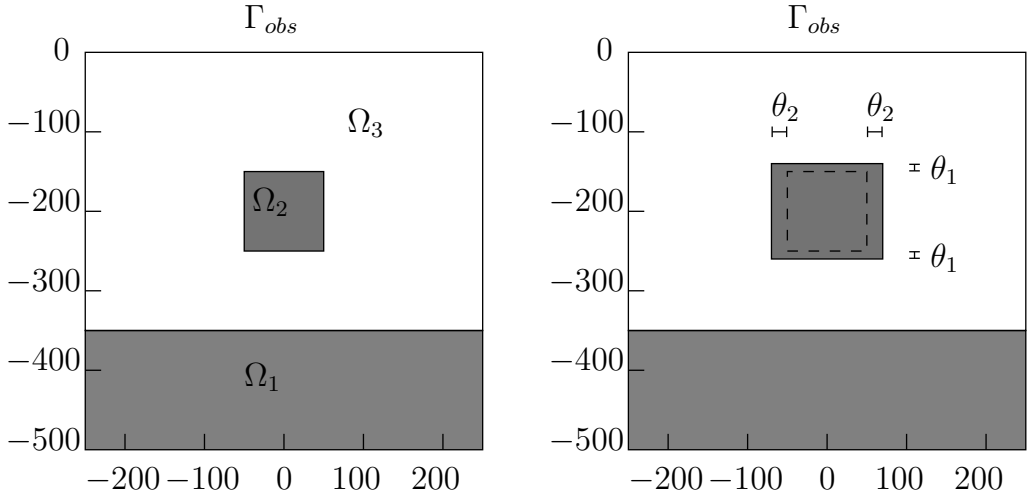

(a) reference domain : $\theta_1 = \theta_2 = 0$ m (b) $\theta_1 = 10$ m , $\theta_2 = 20$ m

Figure 2. First test case: spatial domain (a) and geometric parameterization of the inner interface (b).

where the velocities v_i are expressed in m/s. The squared slowness of σ_3 is constant and is such that $v_3 = \sigma_3^{-1/2} = 2000$ m/s.

Moreover, two geometric parameters, θ_1 and θ_2, determine the height and the width of Ω_2 as follows (Figure 2),

$$\Omega_2 = (-50 - \theta_2, 50 + \theta_2) \times (-250 - \theta_1, -150 + \theta_1) \ ,$$

where distances are in meters.

A homogeneous Robin condition is applied on the bottom and on the two laterals of the domain, while a Neumann condition with value g is applied on the top boundary Γ_{top} with

$$g = \begin{cases} 1 & \text{for } x \in [100, 150] \\ 0 & \text{elsewhere} \end{cases} \ .$$

The choice is made with no loss of generality, due to the linear character of the problem.

A fixed frequency of 15 Hz (corresponding to a minimum wavelength $\lambda_{min} \simeq 133$ m) is considered. Due to the simple geometry of the spatial domain, the coarse mesh used to introduce the geometry parameters into the equation is composed by only $n_T = 18$ macro-elements. The FE mesh, on the other hand, is much finer and it is obtained by subdividing each coarse element into 1024 elements.

Example 1: influence of the sampling points

This first example shows the influence of the different sampling points used to separate $|\mathbf{J}_e|$ and $\mathbf{D}_e$ by the CP algorithm. The two options, as described in Section 3.2, are: i) sampling at FE grid nodes of the parametric meshes, and ii) sampling at the integration points of all FE element of the parametric meshes. Note that ii) prevents one interpolation (from nodes to integration points) when solving the space subproblem of PGD scheme.

In order to test this effect in a simpler setup, only one geometric parameter, θ_1, is considered and the other three parameters are kept fixed with values $\theta_2 = 0$, σ_1 s.t. $v_1 = 4000$ m/s and σ_2 s.t. $v_2 = 2500$ m/s.

Convergence curves of the PGD solution with the number of terms are shown in Figure 3. The relative error plotted are computed as the $L^2(\Omega)$ norm of the difference between the PGD solution and the corresponding FE solution for some particular value of the parameter θ_1.

Copyright © 2010 John Wiley & Sons, Ltd.
Prepared using nmeauth.cls

DOI: 10.1002/nme

Reference values[-]		Computed values[-]		Relative errors [%]		# it
θ_1	θ_2	θ_1	θ_2	θ_1	θ_2	
0.5	0.5	0.50149	0.48318	0.2983	3.3646	52
0.8	0.3	0.79893	0.29862	0.13381	0.45842	56

Table II. Example 4. Results of the parameter identification problem. See caption of Table I for references.

geometric parameters only. Figure 6 show the real part of the solution obtained via PGD and FE for two given sets of parameters values.

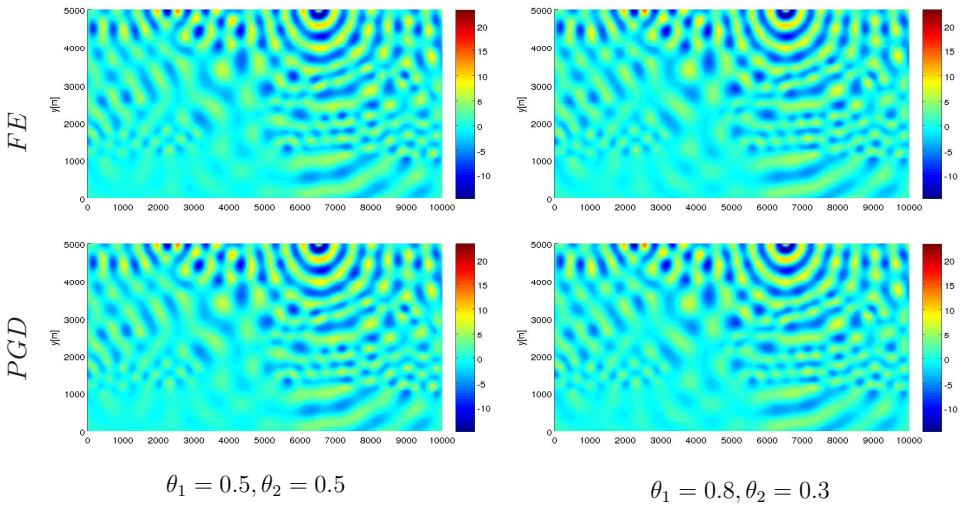

Figure 6. Example 4: Real part of the solution for two sets of geometric parameters. FE solutions (top) and PGD solutions (bottom).

An inverse problem similar to that of the previous section is solved to recover the two parameters. The observed data is again restricted to the surface. Results of recovered parameters are shown in Table II. The relative error of the recovered parameter θ_1 are smaller than those of θ_2. Due to the extremely fast evaluation of the PGD solution, it is possible to plot the functional J in the parameter space, as shown in Figure 7. In that Figure, it can be seen that the functional J is much more sensitive to the first parameter. That explains why the SQP technique can recover θ_1 with smaller errors than θ_2. This ability of the PGD solution to easily estimate the sensitivity on the parameters is extremely helpful to setup efficiently the solver for the inverse problem.

Example 5: inverse problem with geophysical application
The last example consists in the recovery of the geometric and material parameters for the geologic cross section. In addition to the geometric parameters of the previous example, here the squared slowness of the salt (subdomain 1), σ_1, is taken as parameter with values such that the velocity range is $v_1 = \sigma_1^{-1/2} \in (4450, 4700)$.

Results of the inverse problem are shown in Table III. Same as in last example, the sensitivity of θ_2 is lower that that of θ_1. Errors in the recovered parameters are $< 2\%$ for θ_1 and σ_1, while up to 35% for θ_2.

CONCLUSIONS

In this work we apply the PGD technique to a parametric formulation of the Helmholtz problem that is relevant in the context of geological seismic studies. Parameters are of two kinds:

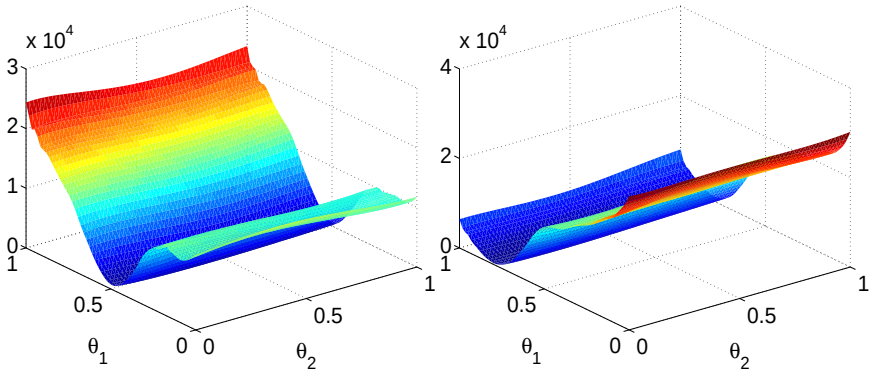

$\theta_1 = 0.5, \theta_2 = 0.5$ $\theta_1 = 0.8, \theta_2 = 0.3$

Figure 7. Example 4: Plot of the functional J in two cases

Reference values			Computed values			Relative errors [%]			# it
[-]		[m/s]	[-]		[m/s]				
θ_1	θ_2	v_1	θ_1	θ_2	v_1	θ_1	θ_2	v_1	
0.8	0.3	4650	0.7967	0.1958	4652.3	0.41	34.7	0.050	114
0.5	0.5	4500	0.5029	0.5637	4509.3	0.59	12.7	0.207	88
0.2	0.6	4550	0.1968	0.5949	4541.9	1.61	0.84	0.179	81

Table III. Example 5. Results of the parameter identification problem. See caption of Table I for references.

material parameters, namely squared slowness of the different materials and geometric parameters, determining the location of internal interfaces between materials.

After the offline phase, PGD allows to obtain in real time the spatial solution for any given set of parameters. This extremely fast response is ideal for the solution of inverse problems, in which the values of the parameters need to be recovered to fit some observed data. The multi-query character (many evaluations of the objective function) of the inverse techniques, makes PGD perfectly suited for that. Moreover, when a global minimum is required, the importance of having a fast forward solver is even bigger, as many inverse problems starting from different initial guesses will be needed, due to the presence of local minima.

Several synthetic examples of the inverse problem presented here show that both kind of parameters can be recovered in most cases with accuracy smaller than $\sim 5\%$. Importantly, the PGD solution allows to easily study the sensitivity of the parameters on the objective function. In this way, it becomes clear when a parameter can or cannot be identified with a given set of observations.

The offline phase of the PDG method requires some algorithmic decisions. Some of them were studied in this work: first, the sampling of the parameter dimensions used to compute the separated Jacobians (required by the geometric parameterization) needs to be done at the integration points in order to avoid interpolation errors that affect the final convergence of the PGD solution. Second, "compressing" PGD solution to reduce its number of terms via a L^2 projection allows to reduce the time of both the online and offline phases. The added computational overhead of the compression step is much smaller than the benefits of keeping the number of terms low.

REFERENCES

1. Symes WW. The seismic reflection inverse problem. *IOPscience* 2009; **25**.
2. Tarantola A. Inversion of seismic reflection data in the acoustic approximation. *Geophysics* 1984; **49**(8):1259–1266.
3. Virieux J, Operto S. An overview of full-waveform inversion in exploration geophysics. *Geophysics* 2009; **74**(6):WCC1–WCC26.
4. Alford RM, Kelly KR, Boore DM. Accuracy of finite-differences modeling of the acoustic wave equation. *Geophysics* 1974; **39**(6):834–842.
5. Plessix RE. A helmholtz iterative solver for 3d seismic-imaging problems. *Geophysics* 2007; **72**(5):SM185–SM194.
6. Song ZM, Williamson PR. Frequency-domain acoustic-wave modeling and inversion of crosshole data: Part 1-2.5-0 modeling method. *Geophysics* 1995; **60**(3):784–795.
7. Kerschen G, Golinval JC, Vakasis AF, Bergman LA. The method of proper orthogonal decomposition for dynamical characterization and order reduction of mechanical systems: An overview. *Nonlinear Dynamics , Springer* 2005; **41**:147–169.
8. Haasdok B, Ohlberger M, Rozza G. A reduced basis method for evolution schemes with parameter-dependent explicit operators. *Electronic Transactions on Numerical Analysis* 2008; **32**:145–161.
9. Chinesta F, Leygue A, Bordeu F, Aguado JV, Cueto E, Gonzalez D, Alfaro I, Ammar A, Huerta A. PGD-Based Computational Vademecum for Efficient Design, Optimization and Control. *Archives of Computational Methods in Engineering* Jan 2013; **20**(1):31–59.
10. Chinesta F, Keunings R, Leygue A. *The Proper Generalized Decomposition for Advanced Numerical Simulations. A Primer*. SpringerBriefs in Applied Sciences and Technology, Springer, 2014.
11. Ammar A, Huerta A, Chinesta F, Cueto E, Leygue A. Parametric solutions involving geometry: a step towards efficient shape optimization. *Computer Methods in Applied Mechanics and Engineering* 2014; **268**:178–193.
12. Zlotnik S, Díez P, Modesto D, Huerta A. Proper generalized decomposition of a geometrically parametrized heat problem with geophysical applications. *Int. J. Numer. Meth. Engng* 2015; **103**(10):737–758.
13. Aguado JV, Huerta A, Chinesta F. R. *International Journal for Numerical Methods in Engineering* 2015; **102**:991–1017, doi:10.1002/nme.4784.
14. Germoso C, Aguado JV, Fraile A, Alarcon E. Efficient PGD-based dynamic calculation of non-linear soil behavior. *Comptes Rendus Mecanique* 2016; **344**:24–41.
15. Nocedal J, Wright S. *Numerical Optimization*. Springer Series, 2006.
16. Mohr M, Kukla PA, Urai JL, Bresser G. Multiphase salt tectonic evolution in nw germany: seismic interpretation and retro-deformation. *Int. J. Earth Sci. (Geol Rundsch)* 2005; (94):917–940.
17. Attanayake J. Seismic migration (sm) 13 November 2006. Presentation.
18. Albertin U, Kapoor J, Randall R, Smith M, Brown G, Soufleris C, Whitfield P, Dewey F, Farnsworth J, Grubitz G, *et al.*. The time for depth imaging. *Oilfield Review* 2002; .
19. Neron D, Ladevèze P. Proper generalized decomposition for multiscale and multiphysics problems. *Archives of Computational Methods in Engineering* 2010; **17**(4):351–372.
20. De Lathauwer L, De Moor B, Vandewalle J. A multilinear singular value decomposition. *SIAM J. Matrix Anal. Appl.* 2000; **21**(4):1253–1278.
21. Carroll JD, Chang JJ. Analysis of individual differences in multidimensional scaling via an n-way generalization of "Eckart-Young" decomposition. *Psychometrika* 1970; **35**(3):283–319.
22. Harshman RA. Foundations of the PARAFAC procedure: Models and conditions for an "explanatory" multimodal factor analysis. *UCLA working papers in phonetics* 1970; **16**:1–84.
23. Modesto D, Zlotnik S, Huerta A. Proper Generalized Decomposition for parameterized helmholtz problems in heterogeneous and unbounded domains: application to harbor agitation. *Comput. Methods Appl. Mech. Eng.* 2015; **295**:127–149, doi:10.1016/j.cma.2015.03.026.
24. Zlotnik S, Díez P, González D, Cueto E, Huerta A. Effect of the separated approximation of input data in the accuracy of the resulting pgd solution. *Advanced Modeling and Simulation in Engineering Sciences* 2015; **2**(28), doi:10.1186/s40323-015-0052-6.
25. Yan F, Han DH, Yao Q, Li H. Seismic velocities of halite salt: anisotropy, dispersion, temperature and stress effects. *SEG* 2014; .

A. SEPARABLE APPROXIMATIONS AND MATRICES

The following separable approximations are introduced for each element $e = 1, \cdots, n_T$ belonging to the coarse mesh :

$$|\boldsymbol{J}_e| \simeq \sum_{l=1}^{n_{Je}} \prod_{j=1}^{n_\theta} T_{\theta_j}^{e,l} \text{ and } \boldsymbol{D}_e \simeq \sum_{a=1}^{3} \sum_{m=1}^{n_{De}^a} \prod_{j=1}^{n_\theta} G_{\theta_j}^{e,a,m} I_a \tag{15}$$

where

$$I_1 = \begin{bmatrix} 1 & 0 \\ 0 & 0 \end{bmatrix} \quad I_2 = \begin{bmatrix} 0 & 1 \\ 1 & 0 \end{bmatrix} \quad I_3 = \begin{bmatrix} 0 & 0 \\ 0 & 1 \end{bmatrix}$$

The scalar $\tilde{\sigma}_e$, associated with the macro-element T_e, is defined to simplify notation in the matrix formulation (Appendix B),

$$\tilde{\sigma}_e = \begin{cases} 1, & \text{if } \sigma \text{ in } T_e \text{ is described by one of the parameters} \\ \sigma|_{T_e}, & \text{else (if the value of} \sigma \text{in } T_e \text{ is a fixed value)} \end{cases}$$

The following definitions are used in the matrix formulation of the PGD algorithm (Appendix B),

$$M_{\hat{x}} = \int_{\hat{T}} N_{\hat{x}} N_{\hat{x}}^T d\hat{x} \qquad K_{\hat{x}}^a = \int_{\hat{T}} \nabla N_{\hat{x}}^T \cdot (I_a \nabla N_{\hat{x}})\, d\hat{x} \qquad M_{x,e}^R = \mathbb{A}_{\partial T_e} \int_{\Gamma_R \cap \partial T_e} N_x^{1D} (N_x^{1D})^T dx$$

$$M_{\theta_j}^{e,l} = \int_{I_{\theta_j}} T_{\theta_j}^{e,l} N_{\theta_j} N_{\theta_j}^T d\theta_j \qquad M_{\theta_j}^{e,a,m} = \int_{I_{\theta_j}} G_{\theta_j}^{e,a,m} N_{\theta_j} N_{\theta_j}^T d\theta_j \qquad M_{\theta_j} = \int_{I_{\theta_j}} N_{\theta_j} N_{\theta_j}^T d\theta_j$$

$$M_{\sigma_s}^e = \int_{I_{\sigma_s}} \left[\sigma_s \tilde{\delta}_{se} + (1 - \tilde{\delta}_{se})\right] N_{\sigma_s} N_{\sigma_s}^T d\sigma_s \qquad M_{\sqrt{\sigma_s}}^e = \int_{I_{\sigma_s}} \left[\sqrt{\sigma_s} \tilde{\delta}_{se} + (1 - \tilde{\delta}_{se})\right] N_{\sigma_s} N_{\sigma_s}^T d\sigma_s$$

$$M_{\sigma_s} = \int_{I_{\sigma_s}} N_{\sigma_s} N_{\sigma_s}^T d\sigma_s$$

$$\mathbf{q}_{x,e} = \mathbb{A}_{\partial T_e} \int_{\Gamma_N \cap \partial T_e} g(x) N_x^{1D} dx \qquad \mathbf{q}_{\theta_j} = \int_{I_{\theta_j}} N_{\theta_j} d\theta_j \qquad \mathbf{q}_{\sigma_s} = \int_{I_{\sigma_s}} N_{\sigma_s} d\sigma_s$$

where $\tilde{\delta}_{se}$ is defined as

$$\tilde{\delta}_{se} = \begin{cases} 1 & \text{the parameter } \sigma_s \text{ describes the material properties of } T_e \\ 0 & \text{otherwise} \end{cases}.$$

B. MATRIX FORMULATION OF THE DISCRETE PROBLEM

The matrix formulation of the alternated directions scheme is described in the Algorithm 1. Unknowns are denoted by $\mathbf{f}_\star$ instead of by $\mathbf{f}_\star^n$. All the matrices and vectors used in the algorithm are defined next. Appendix A presents the definition of all the local matrices and vectors. Let us recall that the symbol $\mathbb{A}$ stands for the matrix assembling operator.

The following matrices and vectors appear in the discrete version of the parametric problem.

$$\begin{aligned} \mathbf{M}_x^{\tilde{m}} = \mathbb{A}_{e=1}^{n_T} \Bigg\{ & -\omega^2 \left[\tilde{\sigma}_e M_{\hat{x}} \left(\sum_{l=1}^{n_{Je}} \prod_{j=1}^{n_\theta} (\mathbf{f}_{\theta_j}^{\tilde{m}})^H M_{\theta_j}^{e,l} \mathbf{f}_{\theta_j}^{\tilde{m}} \right) \prod_{s=1}^{n_\sigma} (\mathbf{f}_{\sigma_s}^{\tilde{m}})^H M_{\sigma_s}^e \mathbf{f}_{\sigma_s}^{\tilde{m}} \right] \\ & + \sum_{a=1}^{3} \left(K_{\hat{x}}^a \sum_{m=1}^{n_{De}^a} \prod_{j=1}^{n_\theta} (\mathbf{f}_{\theta_j}^{\tilde{m}})^H M_{\theta_j}^{e,a,m} \mathbf{f}_{\theta_j}^{\tilde{m}} \right) \prod_{s=1}^{n_\sigma} (\mathbf{f}_{\sigma_s}^{\tilde{m}})^H M_{\sigma_s} \mathbf{f}_{\sigma_s}^{\tilde{m}} \\ & - i\omega \left[\sqrt{\tilde{\sigma}_e} M_{x,e}^R \prod_{j=1}^{n_\theta} (\mathbf{f}_{\theta_j}^{\tilde{m}})^H M_{\theta_j} \mathbf{f}_{\theta_j}^{\tilde{m}} \prod_{s=1}^{n_\sigma} (\mathbf{f}_{\sigma_s}^{\tilde{m}})^H M_{\sqrt{\sigma_s}}^e \mathbf{f}_{\sigma_s}^{\tilde{m}} \right] \Bigg\} \end{aligned} \tag{16a}$$

Algorithm 1: Matrix formulation of the alternated directions scheme

% Computation of p^{n}_{PGD} given p^{n-1}_{PGD}
Input: $\mathbf{f}_x^m$, $\mathbf{f}_{\theta_j}^m$ and $\mathbf{f}_{\sigma_s}^m$ for $j = 1, \cdots, n_\theta$, $s = 1, \cdots, n_\sigma$ and $m = 1, \cdots, n-1$
Initialize $\mathbf{f}_x$, $\mathbf{f}_{\theta_j}$ and $\mathbf{f}_{\sigma_s}$
while *the convergence is not reached, i.e. some* $\mathbf{f}_\star$ *is not yet stationary* **do**
  $[\star = x]$: update $\mathbf{f}_x$ such that

$$\mathbf{M}_x \mathbf{f}_x = \mathbf{r}_x \ ,$$

  where $\mathbf{M}_x = \mathbf{M}_x^n$, and $\mathbf{M}_x^{\tilde{m}}$, $\mathbf{r}_x$ are defined in (16a),(17a)
  for $\tilde{\jmath} = 1, \cdots n_\theta$ **do**
    $[\star = \theta_{\tilde{\jmath}}]$: update $\mathbf{f}_{\theta_{\tilde{\jmath}}}$ such that

$$\mathbf{M}_{\theta_{\tilde{\jmath}}} \mathbf{f}_{\theta_{\tilde{\jmath}}} = \mathbf{r}_{\theta_{\tilde{\jmath}}} \ ,$$

    where $\mathbf{M}_{\theta_{\tilde{\jmath}}} = \mathbf{M}_{\theta_{\tilde{\jmath}}}^n$, and $\mathbf{M}_{\theta_{\tilde{\jmath}}}^{\tilde{m}}$, $\mathbf{r}_{\theta_{\tilde{\jmath}}}$ are defined in (16b),(17b)
  for $\tilde{s} = 1, \cdots n_\sigma$ **do**
    $[\star = \theta_{\tilde{s}}]$: update $\mathbf{f}_{\sigma_{\tilde{s}}}$ such that

$$\mathbf{M}_{\sigma_{\tilde{s}}} \mathbf{f}_{\sigma_{\tilde{s}}} = \mathbf{r}_{\sigma_{\tilde{s}}} \ ,$$

    where $\mathbf{M}_{\sigma_{\tilde{s}}} = \mathbf{M}_{\sigma_{\tilde{s}}}^n$, and $\mathbf{M}_{\sigma_{\tilde{s}}}^{\tilde{m}}$, $\mathbf{r}_{\sigma_{\tilde{s}}}$ are defined in (16c),(17c)
  Check stationarity: |updated $\mathbf{f}_\star$ − previous $\mathbf{f}_\star^{old}$| < tolerance

$$\begin{aligned}
\mathbf{M}_{\theta_{\tilde{\jmath}}}^{\tilde{m}} = \sum_{e=1}^{n_T} \Bigg\{ & -\omega^2 \left[\tilde{\sigma}_e (\mathbf{f}_{x,e}^{\tilde{m}})^H M_{\hat{x}} \mathbf{f}_{x,e}^{\tilde{m}} \sum_{l=1}^{n_{J^e}} \left(\prod_{j \neq \tilde{\jmath}} (\mathbf{f}_{\theta_j}^{\tilde{m}})^H M_{\theta_j}^{e,l} \mathbf{f}_{\theta_j}^{\tilde{m}} \right) M_{\theta_{\tilde{\jmath}}}^{e,l} \prod_{s=1}^{n_\sigma} (\mathbf{f}_{\sigma_s}^{\tilde{m}})^H M_{\sigma_s}^e \mathbf{f}_{\sigma_s}^{\tilde{m}} \right] \\
& + \sum_{a=1}^{3} \left((\mathbf{f}_{x,e}^{\tilde{m}})^H K_{\hat{x}}^a \mathbf{f}_{x,e}^{\tilde{m}} \sum_{m=1}^{n_{D^e}^a} \left(\prod_{j \neq \tilde{\jmath}} (\mathbf{f}_{\theta_j}^{\tilde{m}})^H M_{\theta_j}^{e,a,m} \mathbf{f}_{\theta_j}^{\tilde{m}} \right) M_{\theta_{\tilde{\jmath}}}^{e,a,m} \right) \prod_{s=1}^{n_\sigma} (\mathbf{f}_{\sigma_s}^{\tilde{m}})^H M_{\sigma_s} \mathbf{f}_{\sigma_s}^{\tilde{m}} \\
& - i\omega \left[\sqrt{\tilde{\sigma}_e} (\mathbf{f}_{x,e}^{\tilde{m}})^H M_{x,e}^R \mathbf{f}_{x,e}^{\tilde{m}} \left(\prod_{j \neq \tilde{\jmath}} (\mathbf{f}_{\theta_j}^{\tilde{m}})^H M_{\theta_j} \mathbf{f}_{\theta_j}^{\tilde{m}} \right) M_{\theta_{\tilde{\jmath}}} \prod_{s=1}^{n_\sigma} (\mathbf{f}_{\sigma_s}^{\tilde{m}})^H M_{\sqrt{\sigma_s}}^e \mathbf{f}_{\sigma_s}^{\tilde{m}} \right] \Bigg\}
\end{aligned} \tag{16b}$$

$$\begin{aligned}
\mathbf{M}_{\sigma_{\tilde{s}}}^{\tilde{m}} = \sum_{e=1}^{n_T} \Bigg\{ & -\omega^2 \left[\tilde{\sigma}_e (\mathbf{f}_{x,e}^{\tilde{m}})^H M_{\hat{x}} \mathbf{f}_{x,e}^{\tilde{m}} \sum_{l=1}^{n_{J^e}} \prod_{j=1}^{n_\theta} (\mathbf{f}_{\theta_j}^{\tilde{m}})^H M_{\theta_j}^{e,l} \mathbf{f}_{\theta_j}^{\tilde{m}} \left(\prod_{s \neq \tilde{s}} (\mathbf{f}_{\sigma_s}^{\tilde{m}})^H M_{\sigma_s}^e \mathbf{f}_{\sigma_s}^{\tilde{m}} \right) M_{\sigma_{\tilde{s}}}^e \right] \\
& + \sum_{a=1}^{3} \left((\mathbf{f}_{x,e}^{\tilde{m}})^H K_{\hat{x}}^a \mathbf{f}_{x,e}^{\tilde{m}} \sum_{m=1}^{n_{D^e}^a} \prod_{j=1}^{n_\theta} (\mathbf{f}_{\theta_j}^{\tilde{m}})^H M_{\theta_j}^{e,a,m} \mathbf{f}_{\theta_j}^{\tilde{m}} \right) \left(\prod_{s \neq \tilde{s}} (\mathbf{f}_{\sigma_s}^{\tilde{m}})^H M_{\sigma_s} \mathbf{f}_{\sigma_s}^{\tilde{m}} \right) M_{\sigma_{\tilde{s}}} \\
& - i\omega \left[\sqrt{\tilde{\sigma}_e} (\mathbf{f}_{x,e}^{\tilde{m}})^H M_{x,e}^R \mathbf{f}_{x,e}^{\tilde{m}} \prod_{j=1}^{n_\theta} (\mathbf{f}_{\theta_j}^{\tilde{m}})^H M_{\theta_j} \mathbf{f}_{\theta_j}^{\tilde{m}} \left(\prod_{s \neq \tilde{s}} (\mathbf{f}_{\sigma_s}^{\tilde{m}})^H M_{\sqrt{\sigma_s}}^e \mathbf{f}_{\sigma_s}^{\tilde{m}} \right) M_{\sqrt{\sigma_{\tilde{s}}}}^e \right] \Bigg\}
\end{aligned} \tag{16c}$$

Vectors definition

$$\mathbf{r}_x = \mathbb{A}_{e=1}^{n_T} \mathbf{q}_{x,e} \prod_{j=1}^{n_\theta} \mathbf{f}_{\theta_j}^H \mathbf{q}_{\theta_j} \prod_{s=1}^{n_\sigma} \mathbf{f}_{\sigma_s}^H \mathbf{q}_{\sigma_s} - \sum_{m=1}^{n-1} \mathbf{M}_x^m \mathbf{f}_x^m \tag{17a}$$

$$\mathbf{r}_{\theta_{\tilde{\jmath}}} = \sum_{e=1}^{n_T} \mathbf{f}_{x,e}^H \mathbf{q}_{x,e} \left(\prod_{j \neq \tilde{\jmath}} \mathbf{f}_{\theta_j}^H \mathbf{q}_{\theta_j} \right) \mathbf{q}_{\theta_{\tilde{\jmath}}} \prod_{s=1}^{n_\sigma} \mathbf{f}_{\sigma_s}^H \mathbf{q}_{\sigma_s} - \sum_{m=1}^{n-1} \mathbf{M}_{\theta_{\tilde{\jmath}}}^m \mathbf{f}_{\theta_{\tilde{\jmath}}}^m \tag{17b}$$

$$\mathbf{r}_{\sigma_{\tilde{s}}} = \sum_{e=1}^{n_T} \mathbf{f}_{x,e}^H \mathbf{q}_{x,e} \prod_{j=1}^{n_\theta} \mathbf{f}_{\theta_j}^H \mathbf{q}_{\theta_j} \left(\prod_{s \neq \tilde{s}} \mathbf{f}_{\sigma_s}^H \mathbf{q}_{\sigma_s} \right) \mathbf{q}_{\sigma_{\tilde{s}}} - \sum_{m=1}^{n-1} \mathbf{M}_{\sigma_{\tilde{s}}}^m \mathbf{f}_{\sigma_{\tilde{s}}}^m \tag{17c}$$